DOI: http://doi.org/10.25728/cs.2022.6.5

ANALYSIS OF STRESS EXPOSURES ON AUTONOMOUS NAVIGATION CONDITIONS IN SEARCH CORRELATION-EXTREME NAVIGATION SYSTEMS

A.I. Alchinov[1] and I.N. Gorokhovsky[2]

[1]Trapeznikov Institute of Control Sciences, Russian Academy of Sciences, Moscow, Russia
[2]Research Center of Topographic and Navigational Support, Central Research Institute No. 27, Moscow, Russia

✉ alchinov46@mail.ru, ✉ gin_box@mail.ru

Abstract. This paper further develops the concept of an applied geographic information system (AGIS) for modeling search correlation-extreme navigation systems (CENSs), which was presented in [4]. As shown below, the AGIS can be configured to perform computational experiments with computer models of the existing CENSs and those undergoing various development stages without programming in universal languages. Strict reliability requirements for CENSs increase the role of testing their computer models under stress exposures. During stress testing, the negative effects of different exposures on autonomous navigation conditions are assessed in application areas. Such exposures are not considered at the CENS design stage (reference point masking, distortion of terrain objects borders, etc.). The exposures that prevent CENSs from performing their tasks effectively (critical exposures) are described. Stability to critical exposures is a strong motivation for improving all CENS elements: sensors of geophysical fields, onboard algorithms, and CENS preparation procedures for performing particular tasks in application areas. The mathematical model of approximation by generalized step functions [4] is used to analyze critical exposures on CENS operation. Computer simulation models of different shooting systems are considered as the most important sources of initial data on the approximated function. The mathematical model of stress exposures on CENSs that match images by the mutual correlation criterion is developed further.

Keywords: search correlation-extreme navigation system, shooting system, computer simulation model, stress exposure, stress testing, approximation of functions, generalized step function, reference image, current image.

INTRODUCTION

An inertial navigation system (INS) is the main means of controlling the spatial position of ground, air, sea, and space objects. This system controls the coordinates, velocity, and angular position of vehicles relative to the vertical position. Autonomy is one of the main advantages of INSs. However, errors in determining navigation parameters increase over time, and INS data must be corrected, e.g., using satellite navigation systems (SNSs). In this case, autonomy, a very important quality of any moving object, actually disappears [1, 2]. For example, search correlation-extreme navigation systems (CENSs) have wider capabilities in this regard, as they use map-matching autonomous navigation methods. Such systems serve to refine off-line information about the location, orientation, and other parameters of a moving object coming from the main navigation system. A control system uses this information to compensate the deviations in the object's motion parameters to follow a given route. Search CENSs check hypotheses about the values of motion parameters by matching the current terrain sector image received by the onboard shooting system with fragments of a reference image of the application area. The reference images are prepared in advance

and stored in the memory of the onboard computer. When searching for a reference image fragment close by content to the current image (in the sense of a closeness function in the onboard algorithm), a regular shift grid of the frame selecting the next fragment of the reference image is used. The hypotheses that the sought parameters have values equal to those at the grid nodes are checked. The hypothesis for which the closeness function achieves maximum is accepted. Global search schemes, gradient methods from the arsenal of numerical optimization methods, and their combinations are often used [3].

Correlation-extreme navigation systems provide:

– orientation relative to the real terrestrial surface without binding to the Earth reference system, occupying a small area "on the air," in air, land, sea, and outer space;

– high-precision autonomous navigation, whose accuracy depends mainly on the accuracy of the maps used and their processing methods;

– high or complete noise immunity and hidden operation without any maintenance or recovery cost for navigational fields;

– no negative impact on the environment.

Correlation-extreme navigation systems belong to the class of the most stable and reliable systems.

In CENSs, image matching involves a set of features describing the reference and current images that are independent of flight routes and the altitudes and angles of approaching the correction area of INSs. These features must be invariant with respect to possible mutual transformations: shifting, rotation, and scaling of images.

According to the analysis of CENSs, methods for determining coordinates based on correlation image matching are used in a pre-known set of directions of motion to a given point, and the target is a terminal point in the form of some zone. The reliable operation of CENSs requires correlation functions sensitive to mutual rotation, shifting, and scaling of compared images. To form a reference image, CENSs have special technologies for processing preliminarily obtained images and maps.

Presently, to form control actions, necessary data are acquired in modern vision systems to correct the current coordinates of aircraft. As a result, the crew avoids several functions on information processing and aircraft control: CENSs use information from many sensors (shooting systems), namely, a television camera, a thermal imager, a lidar (detection of low-visibility objects in bad weather and at night), and a radar. The information coming from these sensors is subjected to filtering and segmentation. Then contours are identified, the most significant objects of the terrain are classified, and the resulting information is processed jointly with cartographic information. Joint processing yields the most detailed information about the operating environment of CENSs; due to combining heterogeneous information, objects are detected and identified with considerably higher reliability [2].

This paper further develops the concept of an applied geographic information system (AGIS) for modeling search correlation-extreme navigation systems (CENSs), which was presented in [4]. With this system, experts on the autonomous navigation of moving objects by map-matching methods will receive an information technology (a) to create computer models of the existing CENSs and those undergoing various development stages without programming in universal languages, (b) adjust their operation in application areas, and (c) perform necessary computational experiments with these models. With a special language implemented in the AGIS CENSs, which is close to the professional language for the subject domain, and a friendly application programming interface, an expert adjusts the system for a particular modeling task, getting access to the ready-made software components and geospatial data he needs.

According to the paper [4], strict reliability requirements for CENSs increase the role of testing their computer models under stress exposures. During stress testing, the negative effects of different exposures on autonomous navigation conditions are assessed in application areas. Such exposures are not considered at the CENS design stage. Critical exposures are the exposures that prevent CENSs from performing their tasks effectively. Revealing critical exposures motivates improving all CENS elements: sensors of geophysical fields, onboard algorithms, and CENS preparation procedures for performing particular tasks in application areas. Two problems, i.e., revealing critical stress exposures on autonomous navigation conditions in a given application area of a CENS and preparing this CENS for operation in this application area, can be formulated in general form within the mathematical model of approximation by generalized step functions proposed in [4]. For details, see Section 1 below. Also, we justify the requirements for software components necessary to test the solution methods for these problems.

As demonstrated in [4], computer simulation models of CENS shooting systems are the source of the initial data on the approximated function in these problems. Section 2 below introduces approaches to building such computer models. The mathematical model of stress exposures on autonomous navigation

conditions proposed in [4] covers a particular case of search CENSs, in which onboard algorithms implement the procedure of matching the reference image (created when preparing a CENS for operation in an application area) and the current image received by a CENS sensor at the application instant. In the mathematical model mentioned, the closeness of two images is measured by their correlation coefficient. In Section 3 of this paper, we build another mathematical model of significantly more effective stress exposures on autonomous navigation conditions in application areas of such CENSs.

1. PREPARING SEARCH CENSS FOR OPERATION IN AN APPLICATION AREA. CRITICAL EXPOSURES ON AUTONOMOUS NAVIGATION CONDITIONS

In this paper, we continue conceptualizing the AGIS CENSs, resting on the mathematical model of adjusting a CENS to operate in a given application area [4]. Let us extend this model considering its relations with critical exposures.

Like in the paper [4], for illustrative clarity and easy comprehension of the main features, we choose the following class of search CENSs. The shooting system captures a scene image S on a terrain section, and the onboard algorithm refines the planned coordinates $d=(X,Y)$ of the aircraft at the shooting instant. These limitations will affect neither the set of CENS variants (and the procedures of their adjustment to perform a particular task in a given application area) covered by the model, nor the generality of the analysis results and their practical importance for the conceptual AGIS CENSs with critical exposures.

According to the traditional approach, the adjustment problem is to prepare appropriate a priori (reference) information of a reference image and record it into the CENS onboard memory. "Appropriate" means that the onboard computer will determine the navigation parameters of the moving object with a given accuracy by comparing such information with the current information from the onboard shooting system upon arrival in the application area. On the other hand, the problem of critical exposures is preventing from achieving this goal. We denote these problems by $\boldsymbol{Z}^+$ and $\boldsymbol{Z}^-$, respectively.

The mathematical statement of the problem $\boldsymbol{Z}^+$ involves the following basic notions of map-matching autonomous navigation:

- The autonomous navigation conditions of the aircraft in an application area of a CENS are defined by a function $f(S):M\to D$, where M is the set of possible images S coming from the shooting system to the onboard algorithm input in a given application area, and D is the set of possible locations $d\in D$ of the aircraft at the shooting instant. This function describes an objectively existing relationship between the image content (the "value" of the "variable" $S\in M$) and the aircraft location $d=(X,Y)\in D$ when the shooting system "fixes the value" S. The properties of this relationship can facilitate or hinder using map-matching autonomous navigation.
- A computer model of the shooting system can be the source of initial information $I_0\{f(S):M\to D\}$ about this function when adjusting a CENS for operation in a given application area. After adaptation to the application area, this model simulates shooting system operation in this area: $I_0\{f(S):M\to D\} = \hat{f}^{-1}(\theta)(d,p): D\times P\to M$, where $\theta\in\Theta$ is a generalized parameter with a constant value for all $d\in D$ and $p\in P$. Adaptation consists in setting this particular "value." Its physical meaning will become clear from further presentation. The generalized parameter $p\in P$, where P is the set of admissible values, corresponds to the disturbing factors considered in the shooting system modeling. Selecting an application area means choosing the sets D and P of admissible values of the refined and disturbing parameters, respectively. Note that the function $\hat{f}^{-1}$ is the inverse of $f(S):M\to D$, and the computer simulation model of the shooting system implements a parametric family of such functions, $\{\hat{f}^{-1}(\theta)\}_{\theta\in\Theta}$.
- The CENS onboard computer can be treated as a technical realization of the parametric family of single-valued functions $\{\hat{f}(\alpha)(S)\}_{\alpha\in A}$, where $\hat{f}(\alpha)(S):M\to\hat{D}$ is a particular function from this family. During the CENS adjustment procedure, this function is uniquely chosen depending on the value of the generalized parameter $\alpha\in A$.

As shown in [4], the elementary piecewise constant (step) functions of one variable can be generalized and used to approximate the functions $f(S):M\to D$. In this case, the partitions of the real axis into segments correspond to the partitions of the image set M into classes. It has been found that it is reasonable to solve some actual problems of CENS by applying hierarchical partitions of the set into classes and subclasses. For generalized step functions with the same number

of subclasses in each class at the same hierarchical partition level, we have [4] the analytical expression

$$\hat{f}(S)=\sum_{i_1=1}^{l}\chi_{i_1}\left(\pi(S)\right)\sum_{i_2=1}^{l_1}\chi_{i_1i_2}\left(\pi_{i_1}(S)\right)\ldots$$

$$\sum_{i_r=1}^{l_r}\chi_{i_1i_2\ldots i_r}\left(\pi_{i_1i_2\ldots i_{r-1}}(S)\right)\hat{d}_{i_1i_2\ldots i_r}.$$

Removing the constraint on the number of subclasses yields

$$\hat{f}(S)=\sum_{i_1=1}^{l}\chi_{i_1}\left(\pi(S)\right)\sum_{i_2=1}^{l_{i_1}}\chi_{i_1i_2}\left(\pi_{i_1}(S)\right)\ldots$$

$$\sum_{i_r=1}^{l_{i_1i_2\ldots i_r}}\chi_{i_1i_2\ldots i_r}\left(\pi_{i_1i_2\ldots i_{r-1}}(S)\right)\hat{d}_{i_1i_2\ldots i_r}. \quad (1)$$

Then the problem $\boldsymbol{Z}^+$ can be formulated as a function approximation problem.

Statement of the problem $\boldsymbol{Z}^+$. *The function $f(S):M\to D$ is defined by the inverse $\hat{f}^{-1}(\theta)(d,p):D\times P\to M$, where the parameter $\theta\in\Theta$ has a constant value for all $d\in D$ and $p\in P$, being uniquely determined by choosing the sets D and P (all possible values of the refined and disturbing parameters, respectively). The parametric family of generalized step functions $\left\{\hat{f}(\alpha)(S)\right\}_{\alpha\in A}$ (2) and an admissible CENS error $\varepsilon>0$ are given. It is required to find $\alpha^*\in A$ such that $\rho_M\left(\hat{f}\left(\alpha^*\right)(S),f(S)\right)\le\varepsilon$, where ρ_M denotes a metric in the space of functions with the domain M and the codomain D.*

Recall that the analysis is temporarily restricted to the set $D\subset R^2$. Therefore, for a fixed image *S*, the system response $\hat{d}$ is correct if $\rho\left(\hat{d},d\right)\le\varepsilon$, where ρ denotes the distance function of two points in the plane R^2.

Critical exposures are planned and implemented due to the following reasons. Suppose that the problem $\boldsymbol{Z}^+$ is solved. Upon arriving at the application area and receiving the image *S*, the system will calculate the value of the function $\hat{f}(\alpha^*)(S)=\hat{d}$ and return it as the response. Let the correct response be *d*; the stress exposure will be critical if its realization ensures $\rho\left(\hat{d},d\right)>\varepsilon$ for all possible input images *S* in this application area. Within map-matching autonomous navigation, the function $f(S):M\to D$ is subjected to the stress exposure; see the representation above. The function $\hat{f}^{-1}(\theta)(d,p):D\times P\to M$ is the data source for choosing the values of the stress exposure parameters. The exposure has the following effect: when solving the problem $\boldsymbol{Z}^+$, we use the "obsolete" data on the autonomous navigation conditions (before the exposure) instead of the current data. We should have used not $\hat{f}^{-1}(\theta)(d,p)$ but $(R\cdot\hat{f}^{-1}(\theta))(d,p)$, where *R* is an operator transforming the obsolete function $\hat{f}^{-1}(\theta)$ into the current one considering the exposure.

Therefore, the problem $\boldsymbol{Z}^-$ can be generally formulated as follows.

Statement of the problem $\boldsymbol{Z}^-$. *The function $f(S):M\to D$ is given by the inverse $\hat{f}^{-1}(\theta)(d,p):D\times P\to M$, where the parameter $\theta\in\Theta$ has a known value. The solution $\hat{f}\left(\alpha^*\right)(S):M\to\hat{D}$ of the corresponding problem $\boldsymbol{Z}^+$ is also known. It is required to find an operator R such that*

$$\rho\left(\hat{f}\left((\alpha^*)(\hat{f}^{-1}(\theta)(d,p))\right),\hat{f}\left(\left(\alpha^*\right)(R\cdot\hat{f}^{-1}(\theta))(d,p)\right)\right)>\varepsilon$$

$$\forall\,(d,p)\in D\times P.$$

Consider a particular case of this problem to clarify the meaning of general expressions and further develop the concept of the AGIS CENSs. In formula (1), let *r* = 2 (the levels of hierarchical partitioning into classes and subclasses) and the preliminary image transformations be excluded from the analysis, i.e., $\pi(S)=S$ and $\pi_{i_1i_2\ldots i_{r-1}}(S)=S$. Then we have:

$$M=\bigcup_{i=1}^{l}K_i,\ \text{where}\ K_m\bigcap K_n=\varnothing\ \forall m,n\in[1,l],\ m\ne n;$$

$$K_i=\bigcup_{j=1}^{l_i}K_{ij},\ \text{where}\ K_{im}\bigcap K_{in}=\varnothing$$

$$\forall i=1,\ldots,l\ \text{ and }\ m,n\in[1,l_i],\ m\ne n;$$

$$\hat{f}(S)=\sum_{i=1}^{l}\chi_i(S)\sum_{j=1}^{l_i}\chi_{ij}(S)\hat{d}_{ij}. \quad (2)$$

The expression (2) can be written in the vector form

$$\hat{f}(S)=\left\langle\boldsymbol{\chi}(S),\hat{\boldsymbol{f}}(S)\right\rangle, \quad (3)$$

where angle brackets denote the scalar product of generalized vectors and

$$\boldsymbol{\chi}(S)=(\chi_1(S),\chi_2(S),\ldots,\chi_l(S)),$$

$$\hat{\mathbf{f}}(S)=\left(\hat{f}_1(S),\hat{f}_2(S),\ldots,\hat{f}_l(S)\right),$$

$$\hat{f}_i(S)=\sum_{j=1}^{l_i}\chi_{ij}(S)\hat{d}_{ij}=\left\langle\boldsymbol{\chi}_i(S),\hat{\mathbf{d}}_i\right\rangle,$$

$$\boldsymbol{\chi}_i(S)=\left(\chi_{i1}(S),\chi_{i2}(S),\ldots,\chi_{il_i}(S)\right),$$

$$\hat{\mathbf{d}}_i = \left(\hat{d}_{i1}, \hat{d}_{i2}, \ldots, \hat{d}_{il_i}\right),$$
$$i = 1, \ldots, l.$$

Note that $\hat{f}_i(S)$ are approximating functions for the contractions of the function $f(S): M \to D$ into the subsets $K_i \in M$.

The vector function $\hat{\mathbf{f}}(S)$ has the coordinatewise representation

$$\hat{\mathbf{f}}(S) = \left(\left\langle \boldsymbol{\chi}_1(S), \hat{\mathbf{d}}_1 \right\rangle, \left\langle \boldsymbol{\chi}_2(S), \hat{\mathbf{d}}_2 \right\rangle, \ldots, \left\langle \boldsymbol{\chi}_l(S), \hat{\mathbf{d}}_l \right\rangle\right).$$

As a result, the expression (3) takes the form

$$\hat{f}(S) = \left\langle \boldsymbol{\chi}(S), \left(\left\langle \boldsymbol{\chi}_1(S), \hat{\mathbf{d}}_1 \right\rangle, \left\langle \boldsymbol{\chi}_2(S), \hat{\mathbf{d}}_2 \right\rangle, \ldots, \left\langle \boldsymbol{\chi}_I(S), \hat{\mathbf{d}}_I \right\rangle\right)\right\rangle. \quad (4)$$

According to (4), only the vector functions $\boldsymbol{\chi}(S)$ and $\boldsymbol{\chi}_i(S)$ depend on the input image. By definition, however, any algorithm for calculating such functions is a recognition algorithm [5]. As proved therein, any recognition algorithm can be represented as applying the recognition operator **B**(*S*) to the image *S* and the decision rule **C**(**B**(*S*)) to the result. Note that recognition algorithms use feature sets of the recognized object, extracting them from the images *S* coming from the shooting system through their prior transformations. Now let us analyze such transformations. In the expression (4), we have

$$\boldsymbol{\chi}(S) = \mathbf{C}\left(\mathbf{B}\left(\pi(S)\right)\right),$$

where:

$\mathbf{B}\left(\pi(S)\right) = \left(b_1(\pi(S), b_2(\pi(S), \ldots, b_l(\pi(S))\right)$, $b_i\left(\pi(S)\right)$ is a numerical measure of the closeness of a given image to a class $K_i \in M$;

$C\left(b_1\left(\pi(S)\right), b_2\left(\pi(S)\right), \ldots, b_l\left(\pi(S)\right)\right) = (c_1, c_2, \ldots, c_l)$, where $c_i \in \{0, 1\}$, $i = 1, \ldots, l$;

$\boldsymbol{\chi}_i(S) = \mathbf{C}_i\left(\mathbf{B}_i\left(\pi(S)\right)\right)$, $\mathbf{B}_i$, and $\mathbf{C}_i$, where $i = 1, \ldots, l$, are described by analogy.

Hence, the AGIS CENSs should include libraries of software components implementing these operators and the preliminary transformations of images at different levels: from refinement and filtering to the scene description on the terrain section shot [6].

We adopt the obtained structure of vector characteristic functions to reveal the structure of the parameters $\alpha \in A$ in the parametric families of generalized step functions $\left\{\hat{f}(\alpha)(S)\right\}_{\alpha \in A}$. The analysis below is restricted to the decision rules **C** and $\mathbf{C}_i$ without parameters (the most common case according to [5]). Then the only parametric families are those of recognizing operators. For $\left\{\left(\mathbf{B}\left(\alpha^B\right)\left(\pi\left(\alpha^\pi\right)(S)\right)\right)\right\}_{\alpha^B \in A^B}$, we have

$$\boldsymbol{\chi}(S) = \mathbf{C}\left(\mathbf{B}\left(\alpha^B\right)\left(\pi\left(\alpha^\pi\right)(S)\right)\right),$$

where:

$$\mathbf{B}\left(\alpha^B\right)\left(\pi\left(\alpha^\pi\right)(S)\right) = \left(b\left(\alpha_1^B\right)(\pi\left(\alpha^\pi\right)(S),$$
$$b\left(\alpha_2^B\right)\left(\pi\left(\alpha^\pi\right)(S)\right), \ldots, b\left(\alpha_l^B\right)\left(\pi\left(\alpha^\pi\right)(S)\right)\right),$$

$b\left(\alpha_i^B\right)\left(\pi\left(\alpha^\pi\right)(S)\right)$ is a numerical parametric measure of the closeness of a given image to a class $K_i \in M$;

$$\mathbf{C}\left(b\left(\alpha_1^B\right)\left(\pi\left(\alpha^\pi\right)(S)\right), b\left(\alpha_2^B\right)\left(\pi\left(\alpha^\pi\right)(S)\right), \ldots,$$
$$b\left(\alpha_l^B\right)\left(\pi\left(\alpha^\pi\right)(S)\right)\right) = (c_1, c_2, \ldots, c_l),$$

where $c_i \in \{0, 1\}$, $i = 1, \ldots, l$.

The parametric families $\left\{\mathbf{B}_i\left(\alpha_i^{B_i}\right)\left(\pi\left(\alpha^\pi\right)(S)\right)\right\}_{\alpha_i^{B_i} \in A_i^{B_i}}$ are described by analogy.

Then the parameter α can be represented by the set

$$\alpha = (\alpha^\pi; \alpha_1^B, \ldots, \alpha_l^B; \alpha_1^{B_1}, \ldots, \alpha_{l_1}^{B_1}; \alpha_1^{B_2}, \ldots, \alpha_{l_2}^{B_2}; \ldots;$$
$$\alpha_1^{B_l}, \ldots, \alpha_{l_l}^{B_l}; \hat{\mathbf{d}}_1, \ldots, \hat{\mathbf{d}}_l). \quad (5)$$

The CENS is adjusted for operation in an application area by determining the particular values of the preliminary transformation parameters α^π and recognizing operators α^B and α_i^B and the set of vectors $\hat{\mathbf{d}}_i$. (The component $\hat{d}_{ij} = \left(\hat{X}_{ij}, \hat{Y}_{ij}\right)$ of some vector $\hat{d}_i$ will be returned by the system as a response for $S \in K_{ij}$.)

Section 2 considers image modeling issues for different CENS shooting systems and different preliminary transformations $\pi\left(\alpha^\pi\right)(S)$ with the parameters α^π as well as the corresponding parametric families of functions $\hat{f}^{-1}(\theta)(d, p): D \times P \to M$, where D and P are the value sets of the navigation parameter refined by CENSs and the disturbing parameter, respectively.

Concluding this section, we analyze the other parameters of the set (5) and the parameters $\theta \in \Theta$ used to adjust the shooting system model for a given application area in the problems $\boldsymbol{Z}^+$ and $\boldsymbol{Z}^-$. Consider the example of single-level partitions into classes and CENSs with image matching under no disturbing parameters p (Fig. 1).

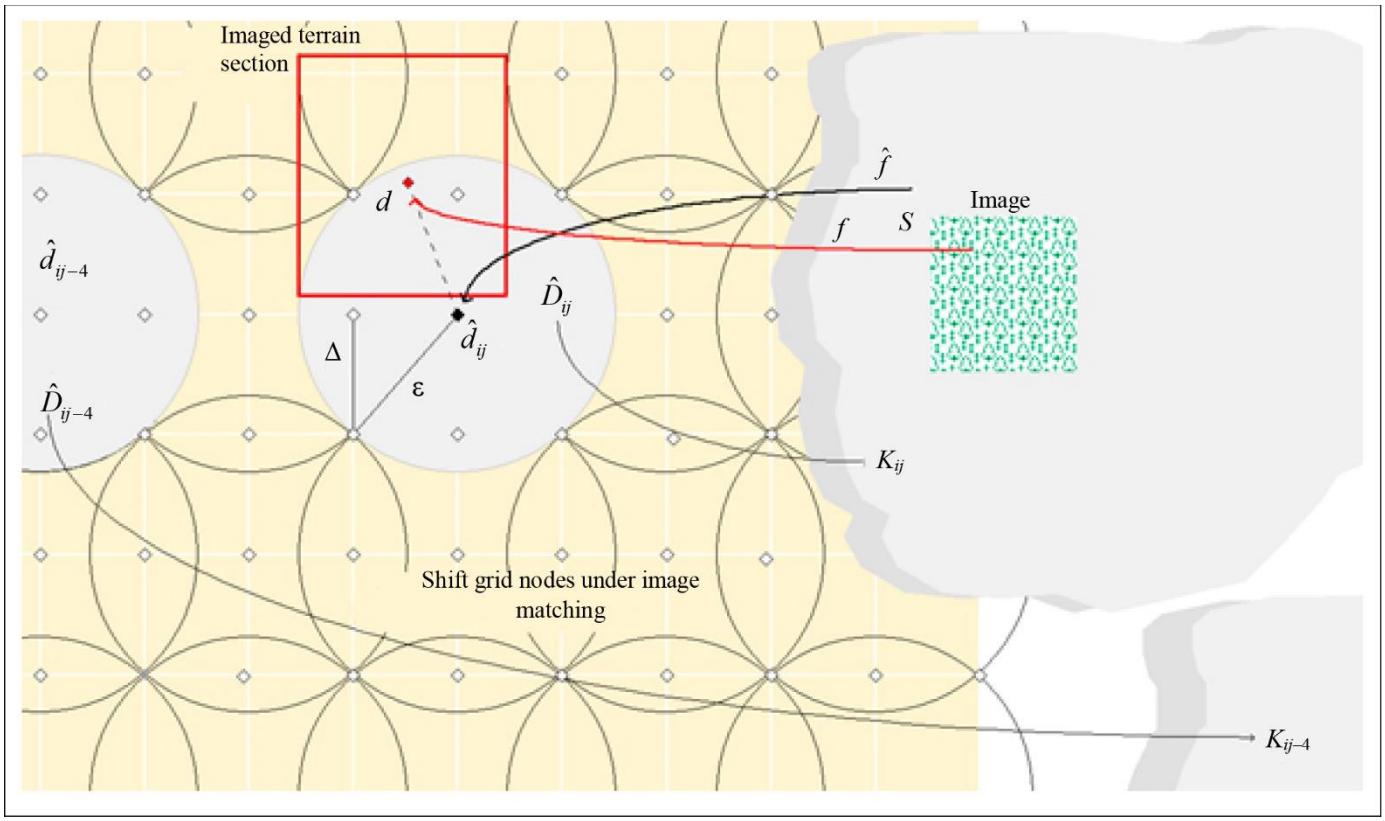

Fig. 1. The notions of the proposed mathematical model.

In this case, the set of possible CENS responses—the nodes of a rectangular grid of shifts—is described by the matrix $\left\|\hat{d}_{ij}\right\| = \left\|\left(\hat{X}_{ij}, \hat{Y}_{ij}\right)\right\|$, where $i = 1, 2, \ldots, m$ and $j = 1, 2, \ldots, n$. The one-level partitioning of the image set M and the expression for the step function take the form

$$M = \bigcup_{i=1}^{m}\bigcup_{j=1}^{n} K_{ij}, \text{ where } K_{ij} \bigcap K_{tq} = \varnothing \ \ \forall i \neq t \text{ and } j \neq q,$$

and

$$\hat{f}(S) = \sum_{i=1}^{m}\sum_{j=1}^{n} \chi_{ij}\left(\pi\left(\alpha^{\pi}\right)(S)\right)\hat{d}_{ij} = \sum_{i=1}^{m}\left\langle \boldsymbol{\chi}_i(S), \hat{\mathbf{d}}_i \right\rangle,$$

where $\boldsymbol{\chi}_i(S) = \left(\chi_{i1}(S), \chi_{i2}(S), \ldots, \chi_{in}(S)\right)$,

$\hat{\mathbf{d}}_i = \left(\hat{d}_{i1}, \hat{d}_{i2}, \ldots, \hat{d}_{in}\right), \ i = 1, \ldots, m.$

With $\boldsymbol{\chi}_i$ written through the superposition of the recognizing operator and the decision rule, we obtain

$$\boldsymbol{\chi}_i(S) = \mathbf{C}_i\left(\mathbf{B}_i\left(\alpha^{B_i}\right)\left(\pi\left(\alpha^{\pi}\right)(S)\right)\right),$$

where:

$$\mathbf{B}_i\left(\alpha^{B_i}\right)\left(\pi\left(\alpha^{\pi}\right)(S)\right) = \left(b_1\left(\alpha_1^{B_i}\right)\left(\pi\left(\alpha^{\pi}\right)(S)\right),\right.$$
$$\left. b_2\left(\alpha_2^{B_i}\right)\left(\pi\left(\alpha^{\pi}\right)(S)\right), \ldots, b_n\left(\alpha_n^{B_i}\right)\left(\pi\left(\alpha^{\pi}\right)(S)\right)\right),$$

$b\left(\alpha_j^{B_i}\right)\left(\pi\left(\alpha^{\pi}\right)(S)\right)$ is a numerical parametric measure of the closeness of a given image to a class $K_{ij} \in M$;

$$\mathbf{C}_i\left(b\left(\alpha_1^{B_i}\right)\left(\pi\left(\alpha^{\pi}\right)(S)\right), \ldots, b\left(\alpha_m^{B_i}\right)\left(\pi\left(\alpha^{\pi}\right)(S)\right)\right) = \left(c_1^i, c_2^i, \ldots, c_m^i\right), \text{ where } c_j^i \in \{0, 1\}, \ j = 1, \ldots, m.$$

Then the parameter α is represented by the set

$$\alpha = (\alpha^{\pi}; \alpha_1^{B_1}, \ldots, \alpha_m^{B_1}; \alpha_1^{B_2}, \ldots, \alpha_m^{B_2}; \ldots; \alpha_1^{B_m}, \ldots, \alpha_m^{B_m}; \hat{\mathbf{d}}_1, \ldots, \hat{\mathbf{d}}_m). \quad (6)$$

A domain is called a shooting area if it combines all terrain sections in the shooting system frame in an application area of a CENS. For a fixed shooting system in the case under consideration, the boundaries of such sections depend only on the planned coordinates of the shooting points.

When solving the problems $\boldsymbol{Z}^+$ and $\boldsymbol{Z}^-$, the partition of the set of possible input images M into classes K_{ij} is supposed to satisfy the following condition: if S belongs to a class K_{ij}, it is obtained in a small neighborhood $\hat{D}_{ij}$ of a node $\hat{d}_{ij}$ of the shift grid $\left\|\hat{d}_{ij}\right\| = \left\|\left(\hat{X}_{ij}, \hat{Y}_{ij}\right)\right\|$, where $i = 1, 2, \ldots, m$ and $j = 1, 2, \ldots, n$. In this case, the CENS error will not exceed ε:

$\rho\left(\hat{d}_{ij},\ d\right) \le \varepsilon = \Delta\sqrt{2}$, where Δ denotes the distance between the grid nodes. Moreover, it is assumed possible to obtain an appropriate reference image (RI) of the shooting area. "Appropriate" means that this image can be used as the parameter $\theta = RI$ of the simulation model of the shooting system $\hat{f}^{-1}(RI)(d): D \to M$ to find the solution (6) of the problem $\boldsymbol{Z}^{+}$ (and solve the problem $\boldsymbol{Z}^{-}$ as well). The first problem consists in calculating the values of the parameters in formula (6) using $\hat{f}^{-1}(RI)(d)$. By assumption, with some preliminary transformation $(\pi(\alpha^{\pi})(S))$, the solutions are $\alpha_j^{B_i} = \hat{f}^{-1}(RI)(\hat{d}_{ij})$ and $\hat{\mathbf{d}}_i = (\hat{d}_{i1},\ldots,\hat{d}_{in})$. The decision rule searches for the maximum value of $b(\alpha_j^{B_i})(\pi(\alpha^{\pi})(S)$ over all i and j and assigns c_j^i a value of 1; for details, see [6, 7].

The formation of reference images satisfying these assumptions is described in Section 2. Section 3 considers the case $b(\alpha_j^{B_i})(\pi(\alpha^{\pi})(S) = \mathbf{r}(\hat{f}^{-1}(RI)(\hat{d}_{ij}), S)$, where $\mathbf{r}$ is the mutual correlation of the image and the reference image fragment corresponding to the shift of the image frame to the node $\hat{d}_{ij}$. For this case, we find an effective operator R solving the problem $\boldsymbol{Z}^{-}$.

2. COMPUTER SIMULATION OF DIFFERENT-TYPE SHOOTING SYSTEMS USED IN CENSS

The correlation image processing algorithm in CENSs is based on maximizing the mutual correlation function C of the current and reference images to decide that at the determination instant the aircraft's coordinates coincide with the reference image center.

Consider control of the value C_1^s during S cycles of stress exposures sequentially introduced in pixels (i, j) of the reference image:

$$C_1^s = \frac{\sum_{i=1}^{Mx}\sum_{j=1}^{My} a_{ij}\left(a_{ij} + \sum_{k=1}^{N} b_k\left(i - x_k, j - y_k\right)\right)}{\sqrt{\sum_{i=1}^{Mx}\sum_{j=1}^{My} a_{ij}^2}\cdot\sqrt{\sum_{i=1}^{Mx}\sum_{j=1}^{My}\left(a_{ij} + \sum_{k=1}^{N} b_k\left(i - x_k, j - y_k\right)\right)^2}}. \quad (7)$$

Here, we use the following notations: a_{ij} is the brightness of the reference image; $a_{ij}\left(a_{ij} + \sum_{k=1}^{N} b_k\left(i - x_k, j - y_k\right)\right)$ is the brightness of the current image (changed by the means of stress exposure by the value b_k in the corresponding pixel (i, j) of the reference image); N is the number of the means of stress exposure; finally, Mx and My are the dimensions of the reference and current images, respectively.

Formula (7) presents the reference and current images. The peculiarities of forming these images and preparing information for the operation of some types of CENS sensors are described below.

The following types of onboard sensors are most developed and widespread.

- Optical sensors in the visible wavelength range of electromagnetic radiation (EMR). The wavelength range of optical radiation is from 100 nm to 1 mm. It is divided into ultraviolet (100–400 nm), visible (400–700 nm), and infrared (700 nm–1 mm); see Fig. 2.
- Thermal sensors in spectral ranges in transparency windows of 0.7–0.9 μm, 0.9–2.5 μm, 3–5 μm, and 8–14 μm (Fig. 2). Thermal sensors have stable operation in the ranges of 3–5 μm and 7–14 μm. CENSs with such sensors work at ranges from a hundred meters to several kilometers.
- Radar sensors in decimeter, centimeter, and millimeter radio bands. They are used mainly to detect ground objects. Active radar sensors can operate at several tens of kilometers but are almost not used for imaging in CENSs. However, there exist many different means with active radar navigation systems, and they can be subjected to stress exposure [8–11].
- Hyper-spectrometers. The development of CENSs with hyper-spectrometers is a priority: multiple information acquisition channels provide real opportunities related to permeability in any environment, reliability of object classification, and selection of interference of natural and artificial origin. In practice, CENSs can implement intelligent positioning of aircraft using modern signal processing methods [12, 13].

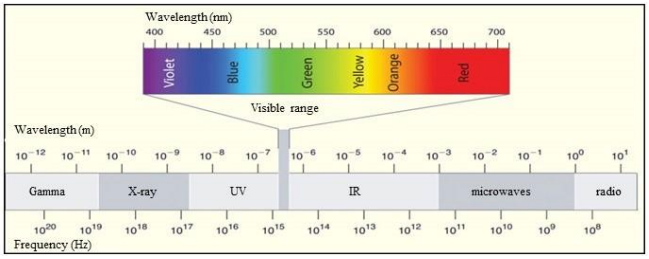

Fig. 2. Radiation ranges.

When creating the unified means of reconnaissance and CENSs, adaptation to a particular task can be carried out by changing the mathematical apparatus of signal processing. Hyperspectral images allow detecting buried and caved objects, minefields, and underground communications due to the significant difference in their reflection spectra. Hyperspectral images display continuous spectral bands, unlike multiband images with separated spectral bands.

CENS sensors of visible and thermal ranges of EMR wavelengths have high spatial and temperature resolution. Radio-thermal CENS sensors provide the resolution necessary for recognizing many areal terrain objects [13].

An important issue is determining the number of the means of stress exposure in the INS correction area. For this purpose, we estimate the accuracy of aircraft navigation using CENSs [5, 8, 9, 14–16]:

$$P_{\text{obj}} = 1 - \exp\left(-\frac{R_{\text{obj}}^2}{2\sigma_{\text{nav}}^2} \right),$$

where P_{obj} is the probability of determining the object's coordinates, R_{obj} is the object's radius on the terrain (in m), and σ_{nav} is the navigation accuracy of the inertial system (in m).

By assumption, an object is detected if the CENS sensor's field of view at least touches the outer boundary of the terrain section where the object is located. The navigation point obeys the Gaussian distribution law, and the lateral deviation and range deviation coincide with one another (Fig. 3).

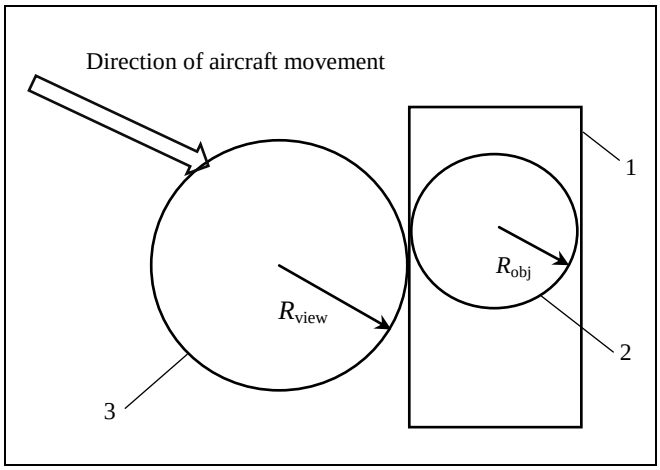

Fig. 3. The sighting scheme for aircraft equipped with CENS at a given point: 1—object location area, 2—the largest radius of the circle fully inscribed in the outer contours of the object, 3—CENS field of view.

When the CENS sensor's field of view (R_{view}) touches the object's location area, particularly the circle of radius R_{obj}, the probability of CENS activation can be supposed 1.

Under the maximum possible errors of the inertial navigation system, the dimensions of the reference image of the terrain must be larger than those of the current image. This condition has not been justified in the available literature. According to [8, 9, 17], the dimensions of the current image obtained by the CENS sensor during navigation can be half the dimensions of the reference image stored in the onboard navigation system.

We emphasize another important aspect. The approach of a moving object to the CENS operation area is guided by the INS and therefore depends on its accuracy. The CENS sensor's field of view on the terrain from the activation altitude must have a radius exceeding three times the mean square error of the INS (σ_{INS}). This requirement ensures position correction by the CENS with a probability close to 1, in accordance with the Gaussian distribution of errors when approaching the object area (under the failure-free operation of the CENS).

If the CENS fails, the accuracy of aircraft navigation will be determined by the accuracy of the inertial navigation system, $\sigma_{\text{nav.}}$ For this purpose, the generated current image should be appropriately modified at the position correction instant by the ground means of stress exposure. Also, they can be placed in the cone of space between the CENS sensor and the object (the circle of radius R_{obj}).

Analysis shows that the expression (7) is sensitive to image distortions and the value C is controllable. Hence, we can propose an optimal method of finding the number and power of the means of stress exposure on the CENS sensor. This method sequentially extracts the brightest or dimmest pixels in the reference image depending on the types of such means.

Methods of purposeful impact on the operation of CENS sensors can reduce their efficiency in modern navigation systems.

Consider the issues of preparing images for use when implementing stress exposure methods for CENSs.

For the areas of stress exposures on the CENS operation, it is necessary to prepare special images by processing photos. A digital image should be partitioned into larger pixels [18]. For example, an original color image of the terrain (Fig. 4) was divided into pixels of dimensions 587×441, and the side length of each pixel of the black-and-white image was 7 m on the terrain (Fig. 5). The following objects were represented in pixel format: a road network (Fig. 6), vegetation (Fig. 7), hydrography (Fig. 8), and a settlement (Fig. 9). These objects are the most informative in the visible range of EMR wavelengths.

The pixel images in Figs. 4–9 have dimensions of 587×441 elements. Each pixel was assigned an average brightness of several pixels of the original image. For preliminary processing, we used a terrain photo consisting of 4241×3769 elements. The side sizes of one pixel were 0.85 m (the original color image on the terrain) and about 7 m (the transformed black-and-white image). These figures are important for further calculations, especially when processing images of large dimensions.

Fig. 4. An original image.

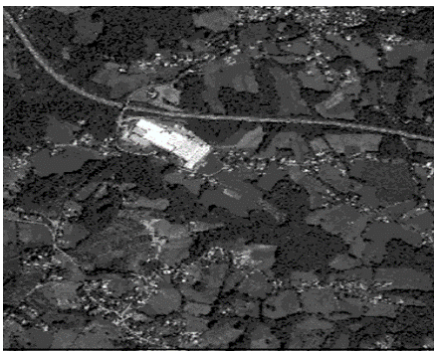

Fig. 5. A black and white image.

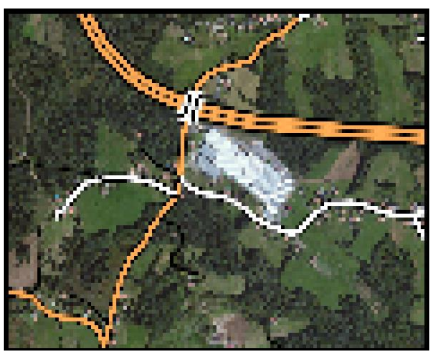

Fig. 6. A road network.

Fig. 7. Vegetation.

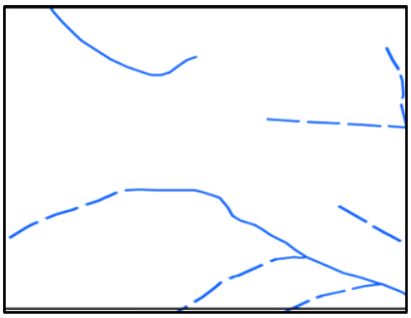

Fig. 8. Hydrography.

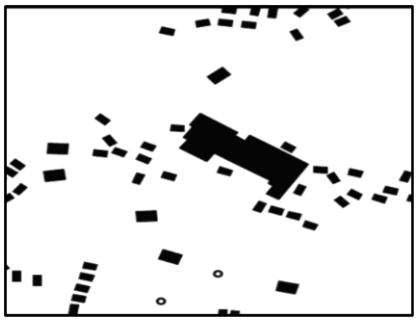

Fig. 9. A settlement.

Figure 5 is a black-and-white image where each pixel shows an optical density value.

This image contains optical density values as the brightness of the reference image (formula (7)). As a rule, the minimum optical density limit does not equal 0: usually, its value is 0.1 conventional units and greater. On the other hand, the maximum limit never equals 4.0: usually, it is less than 3.8. Such ranges can be processed by scanners (e.g., when inputting a digital image). On terrain images, it is possible to display objects with optical densities of 0.1–2.2 and greater. The practice-based scale of these values is presented in the table below.

Tone scale on a black-and-white terrain image

Image phototone	Separation principle	Optical density D
White	Visually distinguishable tone in the image	0.1 or less
Almost white	Optical density of the veil	0.2–0.3
Light gray	Minimum optical density	0.4–0.6
Gray	Average optical density	0.7–1.1
Dark gray	Maximum density	1.2–1.6
Almost black	Tone exceeding the maximum density	1.7–2.2
Black	Visually distinguishable tone of scale	2.2 or more

Figure 10 shows a monochrome image; shades of gray are more likely, but other combinations with tones of one color, such as green-white or green-red, as well as tones from light brown to dark brown, are also possible.

Under digital processing, monochrome has only two values:

– only one color (either on or off), i.e., a binary image;

– shades of this color.

Figure 11 demonstrates a posterized image, specifying the number of tonal levels (brightnesses) of the image. This is necessary, e.g., to create large monotone areas when forming reference images for the subsequent modeling of effective stress exposure conditions for the CENS operation. In all digital images, the color levels are discrete, and the smooth continuous transition between them is achieved by the number of these levels. The black-and-white image in Fig. 12 serves for comparison with the posterized one.

Let us discuss some features of using radar images.

Getting detail at less than 50 cm per pixel is not a challenge for modern satellite radars. However, this resolution applies to only one axis: the pixel will be not square. On the second axis, the resolution could be around 100 cm. For example, 100×25 cm is one of the best current results for the reference image [10]. A radar image is obtained monochrome, with various

Fig. 10. A monochrome image.

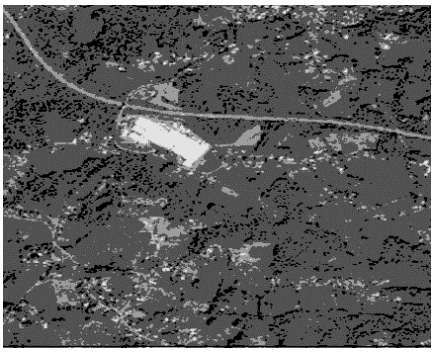

Fig. 11. A posterized image.

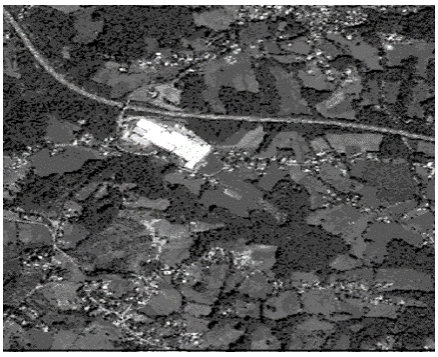

Fig. 12. A black-and-white image.

features of radio waves reflection from different objects, including the display of some details hidden on conventional optical images.

For map-matching navigation systems, we consider the methods and technologies of obtaining and processing satellite photos: other sources are unlikely [3, 11].

When modeling a navigational sensor, a monochrome image most clearly reflects the available reference objects as shades of black or white image fragments, whereas a color image is used only to represent perceived brightness by combining several channels (usually, red, blue, and green). The individual channels can be weighted to achieve the desired result. For example, the green and blue channels can be combined and the red channel can be turned off.

Under hypercube information processing, various representations are possible for the final expressive results in the image, associated with separating the necessary reference objects for CENSs. The reference points should be selected using SURF, one of the most effective modern pattern recognition algorithms [12, 19].

This algorithm includes the following stages:

– performing the scale-space representation,

– calculating the Hessian values,

– searching for local maxima,

– determining the true maximum,

– determining the reference point orientation,

– forming the reference point descriptor.

SURF searches for the key points of the image using the Hessian matrix and creates their descriptors invariant to scale and rotation. The Hessian achieves maximum at the maximum change points of the brightness gradient. It is good at detecting spots, corners, and line edges. The Hessian is invariant to image brightness shift but not to scale. This problem is solved by testing different scales and filters, applying them one by one to a single pixel. The method splits the entire set of scales into octaves.

Different types of images allow choosing objects for managing the computer simulation of CENS performance improvement conditions and CENS failure conditions when the means of stress exposure are applied to onboard motion control programs.

A binary (black and white) image involves only two quantization levels and represents only white and black colors. A grayscale image uses 256 quantization levels, with 8 bits (1 byte) reserved for the description of each image element. Black always corresponds to level 0, whereas white corresponds to level 1 of the binary image and level 255 of the grayscale image.

A color image is formed using a particular palette (RGB, CMYK, etc.). In each palette, colors and their tones are created by mixing the three primary colors in proportions corresponding to their quantization levels.

The RGB palette uses three primary colors: Red, Green, and Blue.

To represent one image element, we need:

– 1 bit for a binary image,

– 8 bits (1 byte) for a grayscale image with 256 quantization levels,

– 24 bits (3 bytes) for a color image with the same number of quantization levels.

When forming an image, the capabilities of onboard CENS computers and their information support are taken into account.

3. OPTIMIZATION OF STRESS EXPOSURES ON AUTONOMOUS NAVIGATION CONDITIONS OF CENSS WITH IMAGE MATCHING BY MUTUAL CORRELATION

Mathematical expressions for calculating automatically the optimal powers of the means of stress exposure located in calculated coordinates were obtained in the paper [4]. As established therein, the means of stress exposure arranged on the terrain (object) have different impacts on the current image formed by the CENS sensor, affecting the similarity of the reference

and current images. By moving the means of stress exposure in a certain installation domain, we can minimize the correlation function of the reference and current images.

Problem statement. *The physical field brightness distribution a_{ij} is known. There are N means of stress exposure on a navigation system sensor, and means k induces a given additional field brightness $b_k(i, j)$ when placed at the origin. Consider a known variant of placing means k at a point with coordinates (x_k, y_k), $k = 1,..., N$. After automatically calculating the optimal powers A_k of each means of stress exposure, it is required to find the displacements $(\Delta x_k, \Delta y_k)$, $k = 1,..., N$, ensuring the reduced correlation between the current and reference images* [10].

Problem solution. In the elementary case, the correlation is calculated on the window $1 \le i \le Mx$, $1 \le j \le My$. Under a given arrangement of the means of stress exposure, the physical field brightness at a point with coordinates (i, j) will be changed means k with power A_k to the value

$$a_{ij} + \sum\nolimits_{k=1}^{N} A_k b_k \left(i - x_k - \Delta x_k, j - y_k - \Delta y_k\right),$$

where: i and j are the pixel coordinates on the reference image; x_k and y_k are the coordinates of the means of stress exposure; Δx_k and Δy_k are the displacements of the means of stress exposure.

The correlation between the current and reference images is given by

$$C = \frac{\sum\limits_{i=1}^{Mx}\sum\limits_{j=1}^{My} a_{ij}\left(a_{ij} + \sum\limits_{k=1}^{N} A_k b_k\left(i - x_k - \Delta x_k,\ j - y_k - \Delta y_k\right)\right)}{\sqrt{\sum\limits_{i=1}^{Mx}\sum\limits_{j=1}^{My} a_{ij}^2} \times \sqrt{\sum\limits_{i=1}^{Mx}\sum\limits_{j=1}^{My}\left(a_{ij} + \sum\limits_{k=1}^{N} A_k b_k\left(i - x_k - \Delta x_k,\ j - y_k - \Delta y_k\right)\right)^2}}. \quad (8)$$

To solve the problem, we find the components of the displacement vector $(\Delta x_1,..., \Delta x_N, \Delta y_1,..., \Delta y_N)$ that decrease the correlation value C. For this purpose, the displacement vector must be opposite to the gradient vector of the function C (the partial derivatives of C in the direction $(\Delta x_1,..., \Delta x_N, \Delta y_1,..., \Delta y_N)$. These partial derivatives are:

$$\frac{\partial C}{\partial \Delta x_s} = \frac{1}{\sqrt{\sum\limits_{i=1}^{Mx}\sum\limits_{j=1}^{My} a_{ij}^2}} \times \left\{ \frac{-\sum\limits_{i=1}^{Mx}\sum\limits_{j=1}^{My} a_{ij} A_s \frac{\partial b_s}{\partial x}\left(i - x_s - \Delta x_s,\ j - y_s - \Delta y_s\right)}{\sqrt{\sum\limits_{i=1}^{Mx}\sum\limits_{j=1}^{My}\left(a_{ij} + \sum\limits_{k=1}^{N} A_k b_k\left(i - x_s - \Delta x_s,\ j - y_s - \Delta y_s\right)\right)^2}} + \right.$$

$$\left. \frac{\left[\sum\limits_{i=1}^{Mx}\sum\limits_{j=1}^{My} a_{ij}\left(a_{ij} + \sum\limits_{k=1}^{N} A_k b_k\left(i - x_k - \Delta x_k,\ j - y_k - \Delta y_k\right)\right) \times \times \sum\limits_{i=1}^{Mx}\sum\limits_{j=1}^{My}\left(A_s \frac{\partial b_s}{\partial x}\left(i - x_s - \Delta x_s,\ j - y_s - \Delta y_s\right) \times \left(a_{ij} + \sum\limits_{k=1}^{N} A_k b_k\left(i - x_k - \Delta x_k,\ j - y_k - \Delta y_k\right)\right)\right)\right]}{\sqrt{\left(\sum\limits_{i=1}^{Mx}\sum\limits_{j=1}^{My}\left(a_{ij} + \sum\limits_{k=1}^{N} A_k b_k\left(i - x_k - \Delta x_k,\ j - y_k - \Delta y_k\right)\right)^2\right)^3}} \right\} =$$

$$\frac{1}{\sqrt{\sum\limits_{i=1}^{Mx}\sum\limits_{j=1}^{My} a_{ij}^2} \times \sqrt{\left(\sum\limits_{i=1}^{Mx}\sum\limits_{j=1}^{My}\left(a_{ij} + \sum\limits_{k=1}^{N} A_k b_k\left(i - x_k - \Delta x_k, j - y_k - \Delta y_k\right)\right)^2\right)^3}} \times$$

$$\left\{ -\sum\limits_{i=1}^{Mx}\sum\limits_{j=1}^{My} a_{ij} A_s \frac{\partial b_s}{\partial x}\left(i - x_s - \Delta x_s,\ j - y_s - \Delta y_s\right) \times \sum\limits_{i=1}^{Mx}\sum\limits_{j=1}^{My}\left(a_{ij} + \sum\limits_{k=1}^{N} A_k b_k\left(i - x_k - \Delta x_k,\ j - y_k - \Delta y_k\right)\right)^2 + \right.$$

$$\left. \sum\limits_{i=1}^{Mx}\sum\limits_{j=1}^{My} a_{ij}\left(a_{ij} + \sum\limits_{k=1}^{N} A_k b_k\left(i - x_k - \Delta x_k,\ j - y_k - \Delta y_k\right)\right) \times \right.$$

$$\sum_{i=1}^{Mx}\sum_{j=1}^{My}\left(A_s \frac{\partial b_s}{\partial x}\left(i-x_s-\Delta x_s,\ j-y_s-\Delta y_s\right)\times\left(a_{ij}+\sum_{k=1}^{N}A_k b_k\left(i-x_k-\Delta x_k,\ j-y_k-\Delta y_k\right)\right)\right)\Bigg\}=$$

$$\frac{1}{\sqrt{\sum_{i=1}^{Mx}\sum_{j=1}^{My}a_{ij}^2}\times\sqrt{\left(\sum_{i=1}^{Mx}\sum_{j=1}^{My}\left(a_{ij}+\sum_{k=1}^{N}A_k b_k\left(i-x_k-\Delta x_k,\ j-y_k-\Delta y_k\right)\right)^2\right)^3}}\times$$

$$\Bigg\{\underline{-\sum_{i=1}^{Mx}\sum_{j=1}^{My}a_{ij}A_s\frac{\partial b_s}{\partial x}\left(i-x_s-\Delta x_s,\ j-y_s-\Delta y_s\right)\times\sum_{i=1}^{Mx}\sum_{j=1}^{My}a_{ij}^2}-$$

$$2\sum_{i=1}^{Mx}\sum_{j=1}^{My}a_{ij}A_s\frac{\partial b_s}{\partial x}\left(i-x_s-\Delta x_s,\ j-y_s-\Delta y_s\right)\times\sum_{i=1}^{Mx}\sum_{j=1}^{My}a_{ij}\sum_{k=1}^{N}A_k b_k\left(i-x_k-\Delta x_k,\ j-y_k-\Delta y_k\right)-$$

$$\sum_{i=1}^{Mx}\sum_{j=1}^{My}a_{ij}A_s\frac{\partial b_s}{\partial x}\left(i-x_s-\Delta x_s,\ j-y_s-\Delta y_s\right)\times\sum_{i=1}^{Mx}\sum_{j=1}^{My}\left(\sum_{k=1}^{N}A_k b_k\left(i-x_k-\Delta x_k,\ j-y_k-\Delta y_k\right)\right)^2+$$

$$\underline{\sum_{i=1}^{Mx}\sum_{j=1}^{My}a_{ij}^2\times\sum_{i=1}^{Mx}\sum_{j=1}^{My}a_{ij}A_s\frac{\partial b_s}{\partial x}\left(i-x_s-\Delta x_s,\ j-y_s-\Delta y_s\right)}+$$

$$\sum_{i=1}^{Mx}\sum_{j=1}^{My}a_{ij}^2\times\sum_{i=1}^{Mx}\sum_{j=1}^{My}\left(A_s\frac{\partial b_s}{\partial x}\left(i-x_s-\Delta x_s,\ j-y_s-\Delta y_s\right)\times\sum_{k=1}^{N}A_k b_k\left(i-x_k-\Delta x_k,\ j-y_k-\Delta y_k\right)\right)+$$

$$\sum_{i=1}^{Mx}\sum_{j=1}^{My}\left(a_{ij}\sum_{k=1}^{N}A_k b_k\left(i-x_k-\Delta x_k,\ j-y_k-\Delta y_k\right)\right)\times\sum_{i=1}^{Mx}\sum_{j=1}^{My}a_{ij}A_s\frac{\partial b_s}{\partial x}\left(i-x_s-\Delta x_s,\ j-y_s-\Delta y_s\right)+$$

$$\sum_{i=1}^{Mx}\sum_{j=1}^{My}\left(a_{ij}\sum_{k=1}^{N}A_k b_k\left(i-x_k-\Delta x_k,\ j-y_k-\Delta y_k\right)\right)\times$$

$$\sum_{i=1}^{Mx}\sum_{j=1}^{My}\left(A_s\frac{\partial b_s}{\partial x}\left(i-x_s-\Delta x_s,\ j-y_s-\Delta y_s\right)\times\sum_{k=1}^{N}A_k b_k\left(i-x_k-\Delta x_k,\ j-y_k-\Delta y_k\right)\right)\Bigg\}=$$

(*By analogy with the paper* [4], *the underlined terms are mutually reduced*.)

$$=\frac{1}{\sqrt{\sum_{i=1}^{Mx}\sum_{j=1}^{My}a_{ij}^2}\times\sqrt{\left(\sum_{i=1}^{Mx}\sum_{j=1}^{My}\left(a_{ij}+\sum_{k=1}^{N}A_k b_k\left(i-x_k-\Delta x_k,\ j-y_k-\Delta y_k\right)\right)^2\right)^3}}\times$$

$$\Bigg\{-2\sum_{i=1}^{Mx}\sum_{j=1}^{My}a_{ij}A_s\frac{\partial b_s}{\partial x}\left(i-x_s-\Delta x_s,\ j-y_s-\Delta y_s\right)\times\sum_{i=1}^{Mx}\sum_{j=1}^{My}a_{ij}\sum_{k=1}^{N}A_k b_k\left(i-x_k-\Delta x_k,\ j-y_k-\Delta y_k\right)-$$

$$\sum_{i=1}^{Mx}\sum_{j=1}^{My}a_{ij}A_s\frac{\partial b_s}{\partial x}\left(i-x_s-\Delta x_s,\ j-y_s-\Delta y_s\right)\times\sum_{i=1}^{Mx}\sum_{j=1}^{My}\left(\sum_{k=1}^{N}A_k b_k\left(i-x_k-\Delta x_k,\ j-y_k-\Delta y_k\right)\right)^2+$$

$$\sum_{i=1}^{Mx}\sum_{j=1}^{My}a_{ij}^2\times\sum_{i=1}^{Mx}\sum_{j=1}^{My}\left(A_s\frac{\partial b_s}{\partial x}\left(i-x_s-\Delta x_s,\ j-y_s-\Delta y_s\right)\times\sum_{k=1}^{N}A_k b_k\left(i-x_k-\Delta x_k,\ j-y_k-\Delta y_k\right)\right)+$$

$$\sum_{i=1}^{Mx}\sum_{j=1}^{My}\left(a_{ij}\sum_{k=1}^{N}A_k b_k\left(i-x_k-\Delta x_k,\ j-y_k-\Delta y_k\right)\right)\times\sum_{i=1}^{Mx}\sum_{j=1}^{My}a_{ij}A_s\frac{\partial b_s}{\partial x}\left(i-x_s-\Delta x_s,\ j-y_s-\Delta y_s\right)+$$

$$\sum_{i=1}^{Mx}\sum_{j=1}^{My}\left(a_{ij}\sum_{k=1}^{N}A_k b_k\left(i-x_k-\Delta x_k,\ j-y_k-\Delta y_k\right)\right)\times$$

$$\sum_{i=1}^{Mx}\sum_{j=1}^{My}\left(A_s\frac{\partial b_s}{\partial x}\left(i-x_s-\Delta x_s,\ j-y_s-\Delta y_s\right)\times\sum_{k=1}^{N}A_k b_k\left(i-x_k-\Delta x_k,\ j-y_k-\Delta y_k\right)\right)\Bigg\}.$$

A similar expression for $\frac{\partial C}{\partial \Delta y_s}$ is obtained by replacing $\frac{\partial b_s}{\partial x}$ with $\frac{\partial b_s}{\partial y}$. The gradient vector in the direction (Δx_1,..., Δx_N, Δy_1,..., Δy_N) gives the displacement vector of the means of stress exposure that reduces the correlation. The displacement value can be calculated by minimizing a function of one variable using the standard bisection algorithm. The iterative application of such displacements allows reducing the correlation at each step. The proposed bisection method is a sequential minimization method for function (8). It is possible to construct nested segments, each containing at least one of the optima (the minimum of the correlation function). There are no such applications of the bisection method, as well as other optimization methods and algorithms for correlation functions, in the available literature. This process continues until achieving a given rate of convergence. Its value is obtained experimentally for each type of CENS sensors during simulation modeling.

The described method can serve to optimize the arrangement of the means of stress exposure in optical, thermal, and radio-thermal wavelength EMR ranges EMI and when using the hypercube of information obtained by hyper-spectrometers in transparency windows. In the radar wavelength range, however, an additional problem arises: the placed means of stress exposure must be oriented in space relative to the field of view of the navigation system sensor so that the reflected signal will return to the system sensor. The means of stress exposure in the radar range are aimed at reducing or increasing the effective scattering surfaces and the distortion of the backward secondary radiation diagram based on reflecting and absorbing composite materials.

CONCLUSIONS

This paper continues studies to justify the project of an applied geographic information system (AGIS) for modeling search correlation-extreme navigation systems (CENSs). The corresponding concept was presented in [4]. Let us summarize the results:

- The mathematical model of approximation of the functions describing autonomous navigation conditions in application areas of search CENSs by generalized step functions has been further developed. This model has been employed to analyze critical stress exposures on the CENS operation. Based on the analysis results, the requirements for the applied geographic information system (AGIS) for the developers of CENSs have been specified.
- Possible dimensions have been determined for the reference image formation area to implement stress testing. Also, the impact of stress testing on the location of the carrier of the map-matching autonomous navigation system has been assessed.
- New procedures have been formulated for the technology of preparing special images with a certain structure. These procedures allow constructing interference zones for onboard sensors, including purposeful impacts to violate the system.
- The arrangement of the means of stress exposure on map-matching autonomous navigation systems with image matching by mutual correlation has been improved.
- Attention has been paid to the use of different physical fields of the Earth in navigation systems. They significantly affect the approaches to stress exposures on the operation of navigation systems.
- The obtained results can be used in technologies for creating modern navigation systems and their testing in complex operating conditions of information sensors in the AGIS CENSs.

REFERENCES

1. Avgustov, L.I., Orientation by Geophysical Fields Provides Autonomous Navigation of Combat Aircraft, *Kommersant-nauka*, 2015, no. 2, pp. 34–35 (In Russian.)
2. Karshakov, E.V., Pavlov, B.V., and Tkhorenko, M.Yu., Promising Map-Aided Aircraft Navigation Systems, *Gyroscopy Navig.*, 2021, vol. 12, no. 1, pp. 38–49. https://doi.org/10.1134/S2075108721010077.
3. Krasovskii, A.A., Beloglazov, I.N., and Chigin, G.P., *Teoriya korrelyatsionno-ekstremal'nykh navigatsionnykh system* (Theory of Correlation-Extreme Navigation Systems), Moscow: Nauka, 1979. (In Russian.)
4. Alchinov, A.I. and Gorokhovsky, I.N., A Conceptual Applied Geographic Information System for Modeling Search Autonomous Correlation-Extreme Navigation Systems, *Control Sciences*, 2022, no. 1, pp. 43–54.

5. Zhuravlev, Yu.I., Zenkin, A.A., Zenkin, A.I., et al., Recognition and Classification Problems with Standard Training Information, *USSR Computational Mathematics and Mathematical Physics*, 1980, vol. 20, no. 5, pp. 195–211.
6. Duda, R.O. and Hart, P.E., *Pattern Classification and Scene Analysis*, Wiley, 1973.
7. Volkovitskiy, A.K., Gladyshev, A.I., Goldin, D.A., et al., A Computer Simulation Complex for Analysis of Magnetic Gradiometry Systems, *Control Sciences*, 2021, no. 3, pp. 57–65.
8. Bolkunov, A.A., Ryazantsev, L.B., and Sidorenko, S.V., Assessment of the Radar Visibility of Armaments, Military and Special Equipment with Using Unmanned Aerial Vehicles, *Voennaya Mysl'*, 2017, no. 9, pp. 70–73. (In Russian.)
9. Likhachev, V.P., Pantyukhin, M.A., and Sidorenko, S.V., An Algorithm for Morphological Processing of Radar Images and Automatic Detection of Objects by Radar Shadow, *Proceedings of Voronezh State Univ. Ser. Syst. Anal. Inform. Tech.*, 2018, no. 2, pp. 150–161.
10. Kupryashkin, I.F., Likhachev, V.P., Seleznev, D.A., and Usov, N.A., A Method to Distort the Radar Image in a Space Radar Station with Synthetic Aperture Antenna, *RF Patent 2622904 RU*, 2017. (In Russian.)
11. *Tekhnicheskie sredstva razvedsluzhb kapitalisticheskikh gosudarstv* (Technical Means of Intelligence Services of Capitalist States), Information Bulletin of All-Russian Institute for Scientific and Technical Information RAS (VINITI), 2009–2015. (In Russian.)
12. Umale, P., Patil, A., Sahani, C., et al., Planer Object Detection Using SURF and SIFT Method, *International Journal of Engineering Applied Sciences and Technology*, 2022, vol. 6, iss. 11, pp. 36–39.
13. Świeżewski, J., YOLO Algorithm and YOLO Object Detection, 2020. URL: https://appsilon.com/object-detection-yolo-algorithm/. (Accessed November 11, 2022.)
14. Abezgauz, G.G., Tron', A.P., Kopenkin, Yu.R., and Korovina, I.A., *Spravochnik po veroyatnostnym raschetam* (Handbook of Probabilistic Calculations), Moscow: Voenizdat, 1970. (In Russian.)
15. Kutakhov, V.P. and Meshcheryakov, R.V., Group Control of Unmanned Aerial Vehicles: A Generalized Problem Statement of Applying Artificial Intelligence Technologies, *Control Sciences*, 2022, no. 1, pp. 55–60.
16. Yuyukin, I.V., Correlation-Extreme Navigation Through Geophysical Fields Based on the Use of Spline Technology, *Vestnik Gos. Univ. Morsk. Rechn. Flota im. Adm. S.O. Makarova*, 2021, vol. 13, no. 4, pp. 505–517. DOI: 10.21821/2309-5180-2021-13-4-505-517. (In Russian.)
17. Antyufeev, V.I., Bykov, V.N., Grichanyuk, A.M., et al., *Matrichnye radiometricheskie korrelyatsionno-ekstremal'nye sistemy navigatsii letatel'nykh apparatov* (Matrix Radiometric Correlation-Extreme Navigation Systems for Aircraft), Kharkov: Shchedraya Usad'ba Plyus, 2014. (In Russian.)
18. Biryukov, V.S., Digital Images in Photogrammetry, *Geodesy and Cartography*, 2000, no. 10, pp. 33–36. (In Russian.)
19. Dyshlyuk, V. O., A Study of Quality and Speed Indicators When Searching for Reference Points on Images by the SURF Method, *Molodoi Uchenyi*, 2018, no. 27 (213), pp. 23–26. (In Russian.)

This paper was recommended for publication by B.V. Pavlov, a member of the Editorial Board.

Received July 12, 2022, and revised November 14, 2022.
Accepted November 29, 2022.

Author information

Alchinov, Alexander Ivanovich. Dr. Sci. (Eng.), Trapeznikov Institute of Control Sciences, Russian Academy of Sciences, Moscow, Russia
✉ alchinov46@mail.ru

Gorokhovsky, Igor Nikolaevich. Dr. Sci. (Eng.), Research Center of Topographic and Navigational Support, Central Research Institute No. 27, Moscow, Russia
✉ gin_box@mail.ru

Cite this paper

Alchinov, A.I., Gorokhovsky, I.N., Analysis of Stress Exposures on Autonomous Navigation Conditions in Search Correlation-Extreme Navigation Systems. *Control Sciences* **6,** 35–48 (2022). http://doi.org/10.25728/cs.2022.6.5

Translated into English by *Alexander Yu. Mazurov*,
Cand. Sci. (Phys.–Math.),
Trapeznikov Institute of Control Sciences,
Russian Academy of Sciences, Moscow, Russia
✉ alexander.mazurov08@gmail.com